Journal Pre-proofs

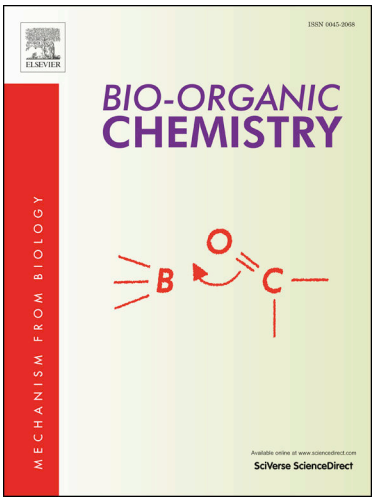

The noncovalent conjugations of bovine serum albumin with three structurally different phytosterols exerted antiglycation effects: A study with AGEs-inhibition, multispectral, and docking investigations

Remah Sobhy, Fuchao Zhan, Enas Mekawi, Ibrahim Khalifa, Hongshan Liang, Bin Li

PII: S0045-2068(19)31189-7
DOI: https://doi.org/10.1016/j.bioorg.2019.103478
Reference: YBIOO 103478

To appear in: *Bioorganic Chemistry*

Received Date: 24 July 2019
Revised Date: 27 October 2019
Accepted Date: 24 November 2019

Please cite this article as: R. Sobhy, F. Zhan, E. Mekawi, I. Khalifa, H. Liang, B. Li, The noncovalent conjugations of bovine serum albumin with three structurally different phytosterols exerted antiglycation effects: A study with AGEs-inhibition, multispectral, and docking investigations, *Bioorganic Chemistry* (2019), doi: https://doi.org/10.1016/j.bioorg.2019.103478

The noncovalent conjugations of bovine serum albumin with three structurally different phytosterols exerted antiglycation effects: A study with AGEs-inhibition, multispectral, and docking investigations

Remah Sobhy[a, c], Fuchao Zhan[a], Enas Mekawi[c], Ibrahim Khalifa[a], Hongshan Liang[a] Bin Li*[a, b]

[a] College of Food Science and Technology, Huazhong Agricultural University, Wuhan, Hubei, 430070, China.

[b] Key Laboratory of Environment Correlative Dietology (Huazhong Agricultural University), Ministry of Education, Wuhan, Hubei, 430070, China.

[c] Department of Biochemistry, Faculty of Agriculture, Benha University, Moshtohor, 13736, Egypt.

*Corresponding author: Prof. Bin Li

College of Food Science and Technology, Huazhong Agricultural University, Wuhan, Hubei, 430070, China,

Tel.: +86 10-82865135,

E-mail: libinfood@mail.hzau.edu.cn

18

19

20 The anti-AGEs effects of 3 structurally different phytosterols were studied.

21 The interaction between stigmasterol, β-sitosterol, and γ-oryzanol with BSA was studied.

22 PS interacted with some of the glycation sites of BSA, e.g. Lys127, 357, 434, 524, and Arg185.

23 PS altered the secondary structures of BSA and showed antiradicals in a Fenton-reaction type.

24 γ-oryzanol highly inhibited the glycation reactions since its structure and antiradical effects.

25

26 **Abstract**

27 The antiglycation effects of three structurally different phytosterols (PS) including stigmasterol,
28 β-sitosterol, and γ-oryzanol on bovine serum albumin (BSA) were deeply studied in a BSA-
29 glucose model by measuring the glycoxidation-based products, SDS-PAGE intensity, free lysine,
30 and their fluorescence microscopy clicks. For the first time, the underlying mechanisms of the
31 antiglycation effects of PS were wholly elucidated by measuring their interaction ability with
32 BSA and their antiradical activity during the glycation reactions. The results showed that PS
33 could partially inhibit the formation of advance glycation end products, block some of the lysyl
34 residues of BSA (Lys127, 357, 434, and 524), prevent the glucose-BAS bonding, and their
35 disaggregation effects on the glycated BSA. Throughout the underlying mechanism behind the
36 antiglycation activity, PS were found to structurally quench the fluorescence intensity of BSA in
37 a static mode, leading to fluctuations in its Z-average size, UV-vis spectrum, and secondary
38 structure. Additionally, PS mitigated the formation the advanced glycation end products by
39 scavenging the radicals produced during the glycation reactions. Overall, these results unleash
40 that PS prevent the glycation reactions and their subsequent changes through shielding the NH_2

groups via H-bonding with their -OH-groups and pi-pi interaction of the steroid core, besides the antiradical activity of PS on the free radicals generating during the glycation reactions.

Keywords: Phytosterols; Bovine serum albumin; Interaction; Multispectral; Molecular docking modeling; Advance glycation end products.

Abbreviations used: Phytosterols (PS); Bovine serum albumin (BSA); Advance glycation end products (AGEs); Stigmasterol (SS); β-sitosterol (βS); and γ-oryzanol (γO).

1. Introduction

Advanced glycation end-products (AGEs) are a group of heterogeneous compounds occurring by bonding of the amino acids with the carbonyl groups of the reducing sugars. The reaction starts by forming the early glycation products, such as Schiff base and Amadori products, which quickly and irreversibly transform to AGEs. AGEs could be also formed under the physiological conditions. The gathering of AGEs is accelerated with some pathophysiological complaints such as diabetes, age-related atherosclerosis, chronic heart failure, Alzheimer's, and some alterations in the protein tissues [1, 2]. Thus, scavenging the progressing of AGEs is critically needed.

The key role of glycations in the development of severe complications and pathological conditions made the recent research was interested on ligand as inhibitors for the non-enzymatic glycation [3]. The synthetic compounds, such as aminoguanidine, have been used as anti-AGEs, although they have austere side-effects which cause non-specific and potentially toxic effects [4, 5]. Due to their side effects, the finding and study of reliable natural inhibitors for the formation of AGEs compounds are needed which will definitely offer impending remediation approaches with fewer side effects [6]. Thus, natural AGEs-inhibitors, such as epicatechin, resveratrol, and many other polyphenols were reported as AGEs inhibitors [7-12]. In addition, some phytosterols (PS), such as β-sitosterol, 31-norcyclolaudenone, and (24R)-4α,14α,4-trimethyl-5 α-cholesta-8,25(27)-dien-3 β-ol were recently gained the attention as a possible natural antiglycation ingredients [13], but the authors only tested their anti-AGEs activity without explaining the underlying mechanisms of their antiglycation effects. Likewise, 31 components (including one phytosterol) were extracted from *Cordia sinensis* leaves showed anti-AGEs effects, but no purified components were used and the underlying mechanisms were not elucidated [14].

Serum albumin (SA) is one of the most abundant soluble plasma proteins in all vertebrates in the

circulatory system in our bodies, and shares approximately half of the total blood proteins. SA has many physiological functions. For example, SA acts as a carrier protein, plays a dominant role in the binding and transport of numerous endogenous and exogenous ligands, and interacts with different biologically active-substances in our bodies [15, 16]. However, SA is highly disposed to the non-enzymatic glycations that significantly alter its secondary structure [17]. As a kind of SA, bovine serum albumin (BSA) is a monomer protein that has 583 amino acid residues, which is often used as uncommon ligand-binding properties, and widely used as a model to study the ligands-proteins binding [18]. Moreover, BSA is extensively used due its similarity with human proteins where 76% of the structure of BSA is similar with human serum albumin [15, 18, 19].

Recently, we found that stigmasterol, β-sitosterol, and γ-oryzanol could show anti-amylolytic effects which could delay the release of glucose and reduce the glycemic level from the source [20]. On the other hand, the increases of the glucose levels have been found to relate with the excessive of the non-enzymatic glycations and accumulation of AGEs [17, 21]. Therefore, this study aimed to analytically investigate the inhibitory effects of stigmasterol, β-sitosterol, and γ-oryzanol, which are the common PS in different plants and foodstuffs [22], on the non-enzymatic early glycation *in vitro* using BSA-glucose models. First, the anti-AGEs effects of each PS were studied by measuring the changes in the fluorescent-AGEs, free lysine, BSA-glucose bond, protein glycoxidation products, SDS-PAGE bands, and the fluorescence microscopy images of BSA-PS-glucose models. Second, the underlying mechanisms of the anti-AGEs of each PS were tested by measuring their interaction with BSA using multidimensional approaches such as dynamic light scattering (DLS), UV-vis absorption, fluorescence quenching, Fourier transform infrared (FTIR), circular dichroism (CD), SDS-PAGE, and computational modeling. Third, the

antiradical effects of each PS during forming the AGEs were also measured in a Fenton-reaction type to gain more details about how PS could mitigate the formation of AGEs. This study will offer a new insight for the potential uses of PS as anti-AGEs natural substances in medication products.

2. Materials and methods

2.1. Chemicals and reagents

Phytosterols (PS) (stigmasterol (SS), β-sitosterol (βS), and γ-oryzanol (γO), HPLC grades, 99% purity) were acquired from Sigma-Aldrich Chemical Co. (St. Louis, MO, USA). Bovine serum albumin (BSA, 98% purity) and aminoguanidine-HCL as a standard antiglycation inhibitor (HPLC-grade) were bought from Yuanye Biotechnology Co., Ltd. (Shanghai, China). D-glucose, methanol, acetic acid, acetone, sodium dodecyl sulfate, and Coomassie brilliant blue R-250 were obtained from Thermo Fisher Scientific Co. (Pittsburg, PA, USA). Deionized water was prepared using MillQ-H_2O system (Millipore, Bedford, MA, USA) which was used in our study to prepare each model [4]. All other chemicals and reagents were of analytical grades.

2.2. Measuring the anti-AGEs effects of PS on a BSA glycated model with glucose

2.2.1. Preparing the BSA-PS-glucose models

The BSA were glycated by glucose (G) to prepare the BSA-G models. First, SS, βS, and γO (0.01, 0.05, 0.1 mg mL^{-1}) were pre-incubated with BSA (30 mg mL^{-1}) for 20 min. After that, the BSA-PS mixtures were glycated using G (20 mM) and the whole mixture was prepared in (PBS, 0.138 M NaCl, 0.0027 M KCl, pH 7.4, 1mM sodium azide as a preservative) at 37 °C to mimic the physiological conditions [23]. We specifically used SS, βS, and γO based on our pre-experiments that showed that these phytosterols have higher antiglycation effects than some of others which were already briefly examined (data not showed). Each sample (5.0 mL) with or

without each PS was incubated in capped 10 mL test tube vials in the dark at 37 °C for 7 d. Aminoguanidine-HCl (0.1 mg mL^{-1}) was used as a control. These samples were used to study the anti-AGEs effects of each PS on BSA.

2.2.2. Measuring the glucose-protein bound and free lysine

The ability of glucose covalently-bind with BSA in BSA-PS-G models was analyzed by phenol-sulphuric acid method [10]. An appropriate dilution of each sample (100 µL) was pipetted into a glass vial with a concentrated sulphuric acid (300 µL) and 60 µL of phenol (5%, v/v). After incubating at 90 °C for 5 min, the samples were cooled to 25 °C for 5 min and scanned at λ = 490 nm using a microplate reader (Multiskan GO, Thermo-Scientific). The consumed glucose was subtracted from the remaining glucose after 7 d of incubation using a standard curve (50-300 µg mL^{-1}) of D-glucose.

The glycation progressing was also determined by measuring free lysine groups using ortho-phthalaldehyde (OPA) method [24]. The OPA-solution was prepared by mixing 25 mL of 0.1 M sodium borate, 2.5 mL of 20% SDS, 100 µL of 2-mercaptpethanol, and 4 mg of OPA, which was dissolved in 1 mL of methanol. The final volume was adjusted to 50 mL with Mill-Q-H_2O. The samples (50 µg proteins) were mixed with 1 mL of OPA-reagent and incubated for 2 min at 37 °C. Absorption was measured at λ = 340 nm against a blank containing OPA-reagent, and the free lysine was calculated based on the standards curve of lysine.

2.2.3. Measuring the fluorescent-AGEs and protein glycoxidation products

The fluorescent-AGEs were detected by measuring the fluorescence intensity of each BSA-PS-G model and the control one at λ_{ex}= 325 and λ_{em}= 440 nm using an F-4600 Luminescence spectrometer at a photomultiplier voltage set of 650 mV and a split set of 10 nm. The fluorescence intensity of the protein glycoxidation products (dityrosine, kynurenine, and N'-

formylkynurenine) was also measured at the wavelengths of 330/415, 365/480, and 325/434 nm, respectively [25].

2.2.4. Sodium dodecyl sulfate-polyacrylamide gel electrophoresis (SDS-PAGE) analysis

SDS-PAGE (12% polyacrylamide gel with 0.1% SDS) analysis was performed to assess the degree of BSA glycation [8]. After incubating each model for 7 d, the reaction solutions were precipitated with the same amount of trichloroacetic acid (10%, v/v). The precipitated glycated protein (10 mg) was collected by centrifugation at 14000g for 20 min. It was then twice washed with cold acetone (5%, v/v), diluted 1:4 (v/v) with Laemmli sample buffer (Bio-Rad Laboratories), and heated at 100 °C for 5 min. After successfully completing the electrophoresis step using a vertical slab gel electrophoresis system (Liuyi, China), the gel was stained by Coomassie Blue R-250 for 4 h and de-stained in a mixture of methanol: acetic acid: MillQ-H2O (3/1/6, v/v/v) solution until the protein bands clearly appeared which were further scanned by an Odyssey Fc Imaging System.

2.2.5. Fluorescence microscopy analysis

The morphology of BSA, BSA-G and BSA-G-□O was observed according to the method of Taha, et al. [26] using a fluorescence microscopy (Nikon Eclipse Ti-S, Nikon Instruments Inc, USA) with X40 objective lens. The fluorescein isothiocyanate (FITC, 0.1%; w/v in DMSO, e_x/e_m= 494/518 nm) and Nile red (0.1%; w/v in EtOH, e_x/e_m = 488-530/ 575-580 nm) were mixed with samples, and images were captured using a camera (Nikon DS-Fi 2.5, Tokyo, Japan).

2.3. Categorizing the binding of BSA-PS mixtures

To study the protein-ligand assembling, the ratio of ligand-protein ratio should be appropriate to measure its influence and evade steric hindrance factor and reduction flocculation [27]. The BSA stock solution was therefore prepared at a concentration of 6×10^{-6} M L^{-1} using the same PBS we

used in the glycation experiments. The stock solution of each PS (5 mg mL^{-1}) was dissolved in a low volume of EtOH (0.5%, v/v) and then the solutions were sonicated (KQ-300DB) to completely dissolving, and diluted with PBS. The amount of ethanol was less than 1% which hardly affect the protein structure [28]. Moreover, each PS with different concentrations were subsequently titrated to give a final concentration of (0.01, 0.05, 0.1 mg mL^{-1}), and kept at 25 °C for 2 h till full equilibrations [18, 20], which were furtherly used to do the spectroscopies-based experiments.

2.3.1. Dynamic light scattering spectroscopy (DLS)

After individually mixing each PS with BSA, each sample was immediately positioned into dust-free cuvettes (1 cm visual path). The measurements were assessed at 25 °C, angle of 173°, and λ= 633 nm using a DLS (Sizer Nano, S5, Malvern, U.K) [20]. Each scan checked 11 runs and the time of each run was 10 s which was triplicated. We used the refractive index of 1.90 which often applied in case of BSA [29]. The Z-average diameter and polydispersity index (PDI) were expressed by non-negative least squares approach.

2.3.2. Ultraviolet spectroscopy (UV-vis)

The UV-vis spectra of BSA and BSA-PS mixtures were scanned using a UV-vis spectroscopy (UV1800, Shimadzu, Japan), in a path-length quartz cuvette (4 mm) with slit width of 1.0 nm at 25 °C and λ= 225-750 nm which was suggested to study the change in the aromatic chromophores environments of proteins [27].

2.3.3. Fluorometric spectroscopy-based measurements

The 2-D fluorescence emission spectra were measured in a quartz cell (1 cm) containing different concentration of each PS with BSA using F-4600 fluorescence spectrometer (Hitachi, Tokyo, Japan) according to Liu et al. [18]. The fluorescence intensity of each BSA-PS mixture

was measured at λ_{ex}= 280 and λ_{em}= 290-450 nm. The excitation and emission slit widths were adjusted at 5 nm with a scanning ratio of 1200 nm min^{-1}. The fluorescence quenching experiments were done at 25, 35, and 45 °C under the same conditions that were used to measure the fluorescence intensity. We also adjusted inner optical filter effect of each PS at λ_{ex}= 280 and λ_{em}= 340 nm [27], then the quenching constants were calculated to get more accurate data. The Stern-Volmer's equation was applied to categorize the fluorescence quenching. The interaction binding constant (K_a) and the number of binding locations (n) were extracted from the y-axis interrupt and the slope of a plot of log [(F_0 - F) / F] versus log [Q], respectively.

2.3.4. Fourier transform infrared spectroscopy (FTIR)

The BSA (6 ×10^{-6} mol L^{-1}) was blended with each PS (0.1 mg mL^{-1}) and lyophilized after 2 h of incubating at 25 °C. The FTIR spectrum of each lyophilized mixture was then recorded using FTIR Nicolet 470 (Thermo Fisher Scientific, USA) using the KBr-disc assay with a ratio of 99:1 of KBr to samples. The spectra were recognized in a transmission mode at 4000 - 400 cm^{-1}, ±2 cm^{-1} resolution, and 21 scans min^{-1}. The FTIR spectra baselines were automatically adjusted and Fourier self-deconvolution was applied using the Omnic software. The whole spectrum of each BSA-PS matrix and the spectral region of 1300-1700 cm^{-1}, which was chosen to evaluate the changes because the amid-I, II, and III bands of the peptide backbone were predicted to be absorbed in this area, were delivered [27]. The second derivative and multiple Gaussian curve-fitting analysis were done using PeakFit software ver. 4.12 (SPSS Inc., Chicago, IL, USA) to estimate the number and place of BSA-bands.

2.3.5. Circular dichroism spectroscopy (CD)

The BSA (6 ×10^{-6} M L^{-1}) solution and its mixture with each PS (0.1 mg mL^{-1}) were prepared using PBS and elevated at 25 °C for 2 h. The Far-UV CD spectra were done using a J-1500

spectrometer (JASCO, Japan) at 25 °C, 0.1 cm visual path quartz cell, λ= 195 - 245 nm, 2 nm bandwidth, 0.5 nm resolution, and a scan velocity of 100 nm min^{-1}. The CD spectra were measured and modified for PBS signal reducing noise and smoothing and expressed as CD ellipticity (mdeg). The secondary structure was analyzed by the SELCON3 assay via DICHROWEB software.

2.3.6. SDS-PAGE

The SDS-PAGE (12% polyacrylamide gel with 0.1% SDS) analysis was performed of each BSA-PS mixture [8]. After incubating each mixture, the reaction solutions were diluted 1:4 (v/v) with Laemmli sample buffer (Bio-Rad Laboratories), and heated at 100 °C for 5 min. An aliquot of each sample (5 μL) and protein molecular weight marker (10-180 kDa) were loaded onto an SDS-PAGE analysis gel (12%). The electrophoresis steps were done using the same procedures as described in section (**2.2.4**).

2.3.7. Molecular docking modeling

The underlying mechanism of the interaction of PS with BSA was consequently elucidated using a docking study. The X-ray structure of BSA (PDB: 3v03) was obtained from the RCSB Protein Data Bank (http://www.rcsb.org/pdb). The chemical structure of SS, βS, and γO was created using Cambridge Soft ChemBioOffice Ultra (Version 14.0) software, and the energy of each structure was approximately minimized with a MM2 job. Subsequently, the structure of each PS was further optimized using Hartree-Fock calculations with the 6-31G (d, p) basis set HF/6-31G (d, p) ** of GAUSSIAN 09 code. The optimized conformations of SS, βS, and γO was separately attached as a ligand **(Fig. 1)**. Before docking, H_2O-molecules were removed and H-atoms were added to BSA-structure using Discovery studio software ver. 2.5 (Accelrys Software Inc, San Diego, CA, USA). Moreover, prior to the molecular docking, we used the site finding tool in

Discovery studio to automatically define and locate the binding sites in the BSA-structure. The site finding tool could recognize the concave regions in the 3D structure of BSA, which were frequently associated with binding events. The binding sites were derived from the cavity within BSA-structure, and we used the BEST method to generate the high-quality conformations. The conjugate-gradient minimization in torsion space and conjugate-gradient as well as Quasi-Newton minimization in Cartesian space were done by the BEST method. The docking simulation was done by the libdock algorithm, which allows full flexibility of small molecules and sets BSA to be rigid. After docking, we used the Discovery studio to analyze and identify the amino acid residues involved in binding.

2.4. Measuring the antiradical activity of PS in BSA-G-•OH media

We also measured the antiradical activity of each PS in a Fenton-reaction type in term of testing the different mechanism possibility of the anti-AGEs effects of each PS we used in our study. First, we prepared the BSA-G model as previously explained (**section 2.2.1**), and then both of $FeCl_2$ (0.4 mM) and H_2O_2 (1 mM) were added and mixed well. After that, 0.1 mg mL^{-1} of the stock solution of SS, βS, and γO was mixed to finally prepare BSA-G-•OH/SS, BSA-G-•OH/βS, and BSA-G-•OH/γO models. After that, each model was filtrated (0.45 μm), filled in a test tube (5 mL), incubated at 37 °C for 7 d, and their AGEs contents were measured at λ_{ex}= 370 nm and λ_{em}= 440 nm [30].

2.5. Statistical analysis

Unless otherwise designated, all experiments were triplicity done. The data were displayed as a mean ± standard deviation which were measured statistically significant when $p<0.05$. The parameters were compared using ANOVA followed by Tukey's multiple assessment post-test using SPSS ver. 22 (IBM, USA). The post-collection data were treated by OriginPro 9.2 (Origin

Lab, Co., USA).

3. Results and discussion

3.1. PS exerted anti-AGEs effects in a BSA-G model

The glycation reactions are initially starting by the covalent binding between reducing sugars and amino acids residues which dramatically consume the available sugars in a medium [31]. Thus, we firstly estimated the early glycation processing using phenol-sulphuric acid method by measuring the levels of glucose covalently-bind to BSA in the BSA-G-PS model. As shown in **Fig. 2A**, glucose was clearly interacted with BSA under the selected glycation conditions we used, showing the starting of the glycation reactions. However, addition of each PS to BSA-G model gradually decreased the glucose-BSA binding ability *in vitro*. For example, 0.1 mg mL^{-1} SS, βS, and γO significantly ($p<0.05$) reduced the glucose which was consumed to bind with BSA by about 23.62, 24.34 and 62.64%, respectively, after 7 d of incubation at 37 °C. Our inhibition values are higher than the inhibition values of ferulic acid which inhabited the glucose-protein binding in BSA and soy glycinin by 17 and 10%, respectively. Generally, the lysine residues have been identified as the major glycation sites of BSA [17]. Therefore, we measured the available lysine to evaluate the blocking and shielding effects of each PS on the lysyl sites of BSA glycated with glucose. As portrayed in **Fig. 2B**, 0.1 mg mL^{-1} of each PS significantly reduced the blocking of free amino groups, directly indicating that the PS could inhibit the creators of the glycation reactions.

The fluorescent intensity could be used to directly measure the AGEs producing after non-enzymatic glycation of proteins. In the BSA-G model, PS inhibited the fluorescent-AGEs creation in a dose dependent-manner. For example, 0.1 mg mL^{-1} of SS, βS, and γO decreased the AGEs-formation by 33.89, 19.64, and 52.44% after 7 d of incubation, respectively (**Fig. 2C**). No

significant differences were found between 0.1 mg mL^{-1} of aminoguanidine and γO, but aminoguanidine was found to significantly inhibit AGEs than SS and βS. However, aminoguanidine showed fainter effects on the proteins glycoxidation products. Aminoguanidine inhibited glucose-mediated formation of AGEs by 31.7%, lower than cyanidin [33] and 60%, equal with linolenic [36]. In a related study, β-sitosterol and 31-norcyclolaudenone extracted from banana flowers inhibited the AGEs by 51.7 and 61.4% in BSA-fructose after 24 h at 50 °C [13], but it should be considered that the incubation conditions and the sugar kind in the media have significant difference on the AGEs-formation [32]. In addition to γO showed higher anti-AGEs effects than many polyphenols such as such as cyanidin (32.9%) [33], wogonoside (47.7%) and luteolin-7 glucoside (49.9%) [2], isoferulic acid (22%) [34], and others. The AGEs-formation are usually accompanied with some glycoxidation products as a result of the oxidation reactions on proteins. Di-tyrosine, kynurenine, and N'-formylkynurenine are common markers for the protein glycoxidation. Di-tyrosine and kynurenine reflect glycoxidative modifications by damaging the Try and Tyr residues of proteins; N'-formylkynurenine is a fluorogenic product of the Try oxidation [25]. It was showed that addition of each PS significantly inhibited the fluorescence intensity of these compounds, and their intensity followed a similar trend as fluorescent AGEs **(Fig. 2C**). However, γO significantly ($p<0.05$) inhibited the fluorescence intensity of the protein glycoxidation products and more than the other PS with inhibition values of 51.31, 12.5, and 56.24% for Di-Tyr, Kyn, and N'-Fkyn, respectively. Similar inhibition values of rosmarinic and carnosic acids in a BSA-G model were recently documented [9].

The glycation reactions could promote the conjugation of BSA-protein to dimer, trimer, and polymer via covalent interacting between the amino residue of proteins and aldehyde groups of sugars. Thus, we used SDS-PAGE analysis to further clarify the shielding effects of each PS on

BSA-modification and oligomerization. Identification of each band was performed by running the samples with a molecular weight marker and the results were also supported by a densitometric analysis of BSA-bands' intensity. As shown in **Fig. 2D**, the first channel with only BSA had a clear band at around 70 kDa (intensity of 14455.45); however, its band intensity was slightly decreased after glycating with G in the absence of PS (channel#2 with intensity of 14153.92). In the presence of PS (channel 3-5), the band intensity of BSA was kept and higher than the glycated BSA without PS, confirming the anti-AGEs effects of each PS in BSA-G models. The inhibition capability of PS could be attributed to its unique structure especially γO compared to other PS, where γO has ferulic acid esterified with sterols ring which increase the -OH groups and the electron delocalization [20]. The glycation reactions could induce structure-changes in the proteins that subsequently promote the protein aggregations. Thus, we furtherly observed the disaggregation effects of γO in BSA-G-γO, BSA-G, and BSA-only models by florescence microscopy, because γO showed the highest anti-AGEs effects. As sown in **Fig. 2E**, the glycated samples showed an increase in the fluorescence intensity which was not observed in the control BSA. Additionally, the glycated BSA showed an accumulation which may be referred to BSA-G aggregates which also hardly appeared in the non-glycated BSA. Most importantly, it was observed that γO had anti-AGEs effects on BSA where the fluorescence intensity was quenched and no BSA-aggregates were found. In agreement with other results, these results give a new sight for PS as anti-glycation and anti-fibrillation impending [35, 36]. Meanwhile, PS can play an important role as anti-amyloid-like fibrillation of BSA (under-investigation). Taken together, these results indicated that PS could inhibit the early and advanced stages of the glycation reactions, and we subsequently elucidated the underlying mechanisms of their anti-AGEs effect by measuring the interaction ability of PS with BSA and

their antiradical activity.

3.2. PS noncovalently interacted with BSA

The particles size spreading is the shortest and/or fastest indicator of the interaction between BSA and other ligands because of their assembling could affect the size of the protein molecules [27]. The DLS was used to examine the hydrodynamic radius of native BSA and each BSA-PS complex. As shown in **Fig. 3**, the BSA solution had Z-average size values of 615 nm. Moreover, the typical size of SS, βS, and γO was around 200-250 nm [20]. Meanwhile, after mixing each PS with BSA, the measured size of BSA-PS mixture was significantly increased ($p<0.05$). Most importantly, γO was found to clearly shift the size of BSA with couple of bands at 825 and up to 1000 nm, probably due to its phenol-sterols conjugates. This is an initial indicator for the creation of PS-BSA mixtures and a new composite appeared to be formed. The PDI ranges of all matrices were lower than 0.5, exemplifying a regular population of masses have been molded.

The fluorescence spectroscopy is a precise technique to study the microenvironment changes in amino acid residues of proteins. Hence, we furtherly used the fluorometric measurements to classify the nature of BSA-PS binding and its underlying mechanism. The fluorescence intensity of BSA is basically derived from the residues of Try (□2) and Tyr (□18) amino acids which could be used to categorize the binding of BSA-PS mixtures and their driving force [41, 42]. As shown in **Fig. 4**, BSA regulated the fluorescence curve direction with a maximum peak at 341 nm after exciting at λ= 280 nm. The fluorescence intensity of BSA was gradually decayed with concentration from 0.01 to 0.1 mg mL^{-1} of each PS, representing the dose-depended effects of PS toward BSA. Moreover, γO significantly ($p<0.05$) inhibited the fluorescence intensity of BSA, followed by SS and βS. For instance, 0.1 mg mL^{-1} of γO, SS, and βS quenched the fluorescence strength of BSA with values of 88.7, 35.60 and 29.59%, respectively, PS has no fluorescence

emission at this wavelength range. These results indicated that each PS could quench the fluorescence of BSA, mainly due their complexation [43]. The different mechanisms of quenching are usually classified as either dynamic or static quenching, which can be distinguished based on their temperature-independent [42]. To classify the quenching mode, we used the Stern-Volmer's plots to experimentally calculate the quenching constants (K_{SV}). The F_0/F plot versus PS concentrations, applying Stern-Volmer's equation, exhibited good linearity ($r^2 > 0.9$) (**Fig. 4**), demonstrating that the ratio of PS to BSA was suitable [27]. As inserted in **Fig. 4**, it could be seen that the Ksv values of PS with BSA declined with increasing temperature, Moreover, the quenching mode (K_q) was also expressed and equated with the highest dispersion scattering collision quenching constant ($2.0 \times 10^{10}\ L^{-1}\ mol^{-1}\ s^{-1}$) which indicated that the fluorescence quenching mechanism was the static one [18]. The rising trend of K_a with increasing temperature was observed, signifying that the capability of each PS binding to BSA were improved and this binding was an endothermic and entropy-driven based-reaction [44]. The n-values were near to 1, implying that there was one binding site on the BSA for PS binding. The binding interaction between micro-ligands with biomolecules can be mainly driven by one or more of the several binding forces which are generally 4 types of forces occur in, viz., H-bonds, van der Waals, hydrophobic, and electrostatic forces. The binding interaction between each PS and BSA can be clarified by the thermodynamic parameters [45]. The negative signal for ΔG° showed that the PS-protein assembling was impulsive. The values of ΔH° and ΔS° of SS, βS, and γO with BSA were of -7.12, -9.24, -13.8 and 4.34, 5.71, 23.54 KJ moL^{-1}, respectively, suggesting that H-bonds and hydrophobic forces played a main role in the binding process [46]. According to the experimental results, PS could potentially exert anti-AGEs effects. PS might interact with BSA even in the presence of glucose, meanwhile PS can exert this protective effect

by competing with glucose for binding with protein residues especially lysine and arginine. Therefore, it seems rational to predicte the binding sites of BSA-PS using docking. The best docking poses of SS-BSA, βS-BSA, and γO-BSA models were portrayed in **Fig. 5A-C**. As found in **Fig. 5A**, SS networked with Lys114, Arg144, Glu125, Glu140, Thr121, Met184, Arg185, Asp118, and Val188 via van der Waals forces. SS interacted with some residues of BSA, namely Pro113, Leu122, Tyr160, Ile141, Pro117, Ile181, Leu115, Asp118, and Lys116 through pi-pi interactions. Results also showed that SS could make H-bonds with Lys127. **Fig. 5B** shows that βS pi-pi interacted with residues of Leu189, Tyr451, Leu454, Ile455, Ala193, His145, Arg144, and Pro110. In addition, Pro113, Lys114, Leu115, Arg185, Thr190, Arg435, Ser428, Lys434, Ser192, Glu424, Arg458, Ser109, and Asp111 were captured by van der Waals with βS. A hydrogen bond was found between βS and Lys375. Likewise, γO interacted with several residues of BSA including Leu574, Phe550, Ala527, Phe508, Phe506, and Lys504 by pi-pi interactions (**Fig. 5C**). While, Leu531, Thr526, Glu530, Phe553, Leu505, Lys127, Lys523, and Thr507 were van der Waals interacted with γO. Most importantly, γO directly interacted with Lys524 via H-bond. The lysine, arginine, and cysteine residues were found as the main sites for the glycosylation of BSA [52], due to their high nucleophilic activities. Lysine-524 was highly noticed as the main glycation site of BSA after glycating with glucose [53]. Thymol declined the glycation of BSA through interacting with some of its glycation sites like Lys524, Arg217, Arg196, and Arg198 [52]. Likewise, sinigrin, linolenic, and isoferulic acids prevent advanced glycation end-products by interacting with Arg194, Arg98, Arg185, Arg198, Arg217, Arg428, Lys190, Lys434, and Lys350 [17, 36, 34]. Our docking study represents that PS could block some of the lysine and arginine sites, such as Lys114, Lys116, Lys127, Lys357, Lys431, Lys504, Lys524, Arg144, Arg185, Arg435, and Arg458. Most importantly, Lys127, Lys357, Lys434,

Lys524, and Arg185 which were considered as the main glycation sites of BSA were interacted with PS. It can block the interaction of glucose with this active site. Because of competitive interaction of glucose and PS to these amino acids, the modifications of arginine and arginine-lysine residues can be prevented using inhibitors. Therefore, attachment of ligand like PS to the amino groups of BSA may inhibit AGEs. In addition, PS interacted with some tyrosine residues such as Tyr451 and Tyr 160 which are responsible for Di-tyrosine, kynurenine, and N'-formylkynurenine oxidation, matching with our experimental findings well. Binding of one PS molecule to BSA is demonstrated in **Fig. 5**. When the concentration of PS is increased, more lysine and arginine amino acids will occupy. According to the experimental results, PS have anti-AGEs in a concentration-dependent manner. The predicted results from the docking approaches have good agreement with the obtained results from the experimental data. It can be concluded that the hydrophobic interaction between PS and residues in the glycation site can be considered as an inhibitory mechanism for this compound. Keep in mind that the binding of ligand-protein was frequently attended by fluctuations in the secondary structure of proteins; to gain a better understanding we also did UV, FTIR, and CD spectroscopies to discover the changes in the structure of BSA-PS mixtures.

3.3. PS altered the secondary structure of BSA

The UV-vis spectroscopy is an effectual tool to study the protein-ligand interactions through analyzing the alterations around the Try and Tyr residues of proteins [37]. The aromatic amino acids donate to bands in the range of 255-300 nm. **Fig. 6** displays the recorded UV-vis absorption spectra of BSA with and/or without SS, βS, and γO. It was clearly showed that BSA had one absorption peak at $\lambda = 282$ nm, which belongs to its Try residue [38]. Most importantly, the maximum peak position of BSA was right-shifted after mixing with the PS, especially γO,

418 indicating to their binding simultaneously and changes nearly to the environment of their Try and
419 Tyr residues were occurred [39]. These results indicated that the interaction between BSA and
420 each PS was happened, probably due to the steroid nucleus attached with -OH group of the late
421 structure that could assemble with BSA. Outstandingly, γO was found to significantly alter the
422 hydrophobicity of the micro-environment of Try and Tyr residues of BSA than the other PS,
423 mainly due to its phenol-sterols conjugates. A recent study reported that the spectral changes of
424 the proteinaceous materials could be happened due to their complexation with other ligands [40].
425 FTIR could be used to explore the changes in the secondary structures of proteins in aqueous
426 solution [16]. The FTIR spectra of BSA showed sum of amide bands, representing various
427 vibrations of the peptide moiety. Amongst these bands, amide I, II, and III bands of FTIR spectra,
428 which separately appeared in the region of 1300 - 1700 cm^{-1} have been extensively used to
429 analyze the proteinaceous materials [47]. As shown in **Fig. 7**, the major 3 peaks of BSA were
430 distinguished at 1504.2, 1444.4, and 1367.3 cm^{-1}, fitting to amid-I (C=O), II (N-H, C-H), and III
431 (N-H), respectively. Inversely, exposure of BSA to 0.1 mg mL^{-1} of each PS shifted the FTIR
432 peak of each amid, showing the gathering between each PS and BSA amides. The C=O band
433 stretching of BSA-PS became broader and deeper than that of BSA alone, signifying the
434 probability that the functional groups of amino acids have been networked with PS. We furtherly
435 fitted the FTIR peak from 1300 to 1700 cm^{-1} to precisely evaluating the secondary structure
436 alteration of BSA affected by PS addition [47]. As supported by peak fitting analysis, the peaks
437 of BSA were shifted especially in the presence of γO, with shifts from 1367.3, 1444.4, and
438 1504.2 to 1365.3, 1452.1, and 1542.7 cm^{-1}, separately. These results disclosed that each PS
439 greatly affected the secondary structure of BSA. To validate the FTIR results, the possible
440 influence of PS on the secondary structure of BSA was analyzed using the CD spectroscopy [48].

As figured in **Fig. 8A**, the far-UV CD spectra of BSA were mainly featured by 2 negative bands at ~208 and 222 nm (typical feature of α-helix in the advanced structure of BSA) resulting from n→π* and π→π* shifts of the amide groups [49]. With addition of each PS, the CD intensity of BSA was fluctuated with remarkable shifts of the peak shapes and positions, representing the partial modifications in the secondary structure of BSA. As shown in **Fig. 8B**, the ratios of the secondary structure elements of BSA were altered after mixing with each PS. For instance, 0.1 mg mL^{-1} of SS increased the α-helical content and decreased the β-sheet of BSA, whereas the opposite actions were happened in the presence of γO. These results disclosed that interaction of each PS with BSA induced an unfolding of the constitutive polypeptides [50]. This proposes that PS may terminate H-bonds in the inner structure of BSA so as to convert its secondary structure. From the CD results it can be concluded that the protein is becoming slightly more compact which agreed with similar results [51]. SDS-PAGE analysis was also used to evaluate the covalent interaction occurred between each PS and BSA. As shown in **Fig. 8C**, 0.1 mg mL^{-1} of SS and γO slightly decreased the SDS-PAGE intensity of BSA-band by about 4.21 and 4.95%, respectively, while βS hardly influence the BSA-band, indicating that each PS could only noncovalent interact with BSA. The aforenoted results suggested that each PS could bind with BSA-structure and induce changes in its secondary structure.

3.4. PS exerted antiradical effects in BSA-G-˙OH models

The active oxygen produced in the process of hydrolysis often accelerates the glycosylation reaction and promotes the formation of AGEs. Therefore, we measured the antiradical ability of each PS in BSA-G models after adding Fe_2^+ and H_2O_2 to simulate the Fenton reaction and generate hydroxyl radicals. As found in **Fig. 9**, ˙OH promoted the producing of AGEs and significantly ($p<0.05$) increased their fluorescence intensity by about 16.87% compared with the

BSA-G model, representing the augmenting role of •OH on AGEs formation. However, adding of 0.1 mg mL^{-1} of SS, βS, and γO reduced the fluorescence intensity of AGEs induced by •OH with values of 18.61, 12.25, and 35.48%, respectively compared with the BSA-G-•OH model. Bayberry polyphenols were also found to inhibit the formation of AGEs by scavenging •OH during the glycation reactions in a similar Fenton-type reaction [30]. These results indicated that PS could also capture the reactive carbonyl intermediates produced during the glycation reactions and subsequently inhibiting the formation of AGEs.

4. Conclusion

The underlying mechanism of the anti-AGEs of PS on BSA were elucidated. It was found that each PS could shield the BSA against the glycation reactions via reducing its binding with the reducing sugars and blocking some of their lysyl sites (the initial step of the glycation reactions) and scavenged the free radicals. SS, βS, and γO also reduced the glycoxidation products of BSA after glycating and kept its SDS-PAGE bands' intensity. The present study unleashes the molecular underlying mechanisms of the anti-AGEs effect of 3 different structure PS on BSA-protein that could be used to formulate functional foods with relatively low AGEs-associated health risk. Compared with SS and βS, γO was a promising inhibitor on AGEs and could be utilized as a potential therapeutic or a functional supplement to reduce the AGEs-levels.

Acknowledgements

The authors gratefully acknowledge the National Key R&D Program of China (Program No. 2017YFD0400205), Technical Innovation Program of Hubei Province (Program No. 2017ABA150), and the Chinese Scholarships Council (No. 2017SLJ023757) for their financial support.

Declaration of Competing Interest

The authors declared that there is no conflict of interest.

Author contributions

RS conceived the main hypothesis, designed, performed all experiments, and wrote the manuscript. FZ assisted in some experiments. IK assisted in the docking experiments. EM, HL, and BL critically proofread the manuscript. All authors read the manuscript.

5. References

[1] S.-R. Yoon, S.-M. Shim, Inhibitory effect of polyphenols in Houttuynia cordata on advanced glycation end-products (AGEs) by trapping methylglyoxal, LWT Food Sci Technol 61(1) (2015) 158-163.

[2] I. Grzegorczyk-Karolak, K. Gołąb, J. Gburek, H. Wysokińska, A. Matkowski, Inhibition of advanced glycation end-product formation and antioxidant activity by extracts and polyphenols from *Scutellaria alpina* L. and *S. altissima* L, Molecules 21(6) (2016) 739.

[3] K.M. Khan, M. Irfan, M. Ashraf, M. Taha, S.M. Saad, S. Perveen, M.I. Choudhary, Synthesis of phenyl thiazole hydrazones and their activity against glycation of proteins, Med Chem Res 24(7) (2015) 3077-3085.

[4] L. Zeng, H. Ding, X. Hu, G. Zhang, D. Gong, Galangin inhibits α-glucosidase activity and formation of non-enzymatic glycation products, Food Chem 271 (2019) 70-79.

[5] K.M. Khan, M. Khan, M. Ali, M. Taha, S. Rasheed, S. Perveen, M.I. Choudhary, Synthesis of bis-Schiff bases of isatins and their antiglycation activity, Bioorg Med Chem 17(22) (2009)

7795-7801.

[6] K. Mohammed Khan, Z. Shah, V. Uddin Ahmad, M. Khan, M. Taha, F. Rahim, H. Jahan, S. Perveen, M. Iqbal Choudhary, Synthesis of 2, 4, 6-trichlorophenyl hydrazones and their inhibitory potential against glycation of protein, Med Chem 7(6) (2011) 572-580.

[7] Y. Hou, Z. Xie, H. Cui, Y. Lu, T. Zheng, S. Sang, L. Lv, Trapping of glyoxal by propyl, octyl and dodecyl gallates and their mono-glyoxal adducts, Food Chem 269 (2018) 396-403.

[8] Y. Shen, Z. Xu, Z. Sheng, Ability of resveratrol to inhibit advanced glycation end product formation and carbohydrate-hydrolyzing enzyme activity, and to conjugate methylglyoxal, Food Chem 216 (2017) 153-160.

[9] J. Ou, J. Huang, M. Wang, S. Ou, Effect of rosmarinic acid and carnosic acid on AGEs formation in vitro, Food Chem 221 (2017) 1057-1061.

[10] J.M. Silván, S.H. Assar, C. Srey, M.D. Del Castillo, J.M. Ames, Control of the Maillard reaction by ferulic acid, Food Chem 128(1) (2011) 208-213.

[11] X. Li, T. Zheng, S. Sang, L. Lv, Quercetin inhibits advanced glycation end product formation by trapping methylglyoxal and glyoxal, J. Agric. Food Chem 62(50) (2014) 12152-12158.

[12] M.M. Alam, I. Ahmad, I. Naseem, Inhibitory effect of quercetin in the formation of advance glycation end products of human serum albumin: An *in vitro* and molecular interaction study, Int. J. Biol. Macromol 79 (2015) 336-343.

[13] Z. Sheng, H. Dai, S. Pan, B. Ai, L. Zheng, X. Zheng, W. Prinyawiwatkul, Z. Xu, Phytosterols in banana (*Musa spp*.) flower inhibit α-glucosidase and α-amylase hydrolysations and glycation reaction, Int J Food Sci Tech 52(1) (2017) 171-179.

[14] K. Khan, M. Rasheed, M. Nadir, S. Firdous, S. Faizi, GC-MS & preliminary screening

533 profile of *Cordia sinensis* leaves – antiglycation, antifungal and insecticidal agents, Nat Prod Res
534 (2019) 1-5.
535 [15] A.S. Roy, D.R. Tripathy, A. Chatterjee, S. Dasgupta, A spectroscopic study of the
536 interaction of the antioxidant naringin with bovine serum albumin, Biophys. Chem 1(03) (2010)
537 141.
538 [16] S. Cao, D. Wang, X. Tan, J. Chen, Interaction between trans-resveratrol and serum albumin
539 in aqueous solution, J Solution Chem 38(9) (2009) 1193-1202.
540 [17] S. Awasthi, N.T. Saraswathi, Sinigrin, a major glucosinolate from cruciferous vegetables
541 restrains non-enzymatic glycation of albumin, Int. J. Biol. Macromol 83 (2016) 410-415.
542 [18] J. Liu, Y. He, D. Liu, Y. He, Z. Tang, H. Lou, Y. Huo, X. Cao, Characterizing the binding
543 interaction of astilbin with bovine serum albumin: a spectroscopic study in combination with
544 molecular docking technology, RSC Advances 8(13) (2018) 7280-7286.
545 [19] N. Zhou, Y.-Z. Liang, P. Wang, 18β-Glycyrrhetinic acid interaction with bovine serum
546 albumin, J Photoch Photobio A 185(2-3) (2007) 271-276.
547 [20] R. Sobhy, M. Eid, F. Zhan, H. Liang, B. Li, Toward understanding the *in vitro* anti-
548 amylolytic effects of three structurally different phytosterols in an aqueous medium using
549 multispectral and molecular docking studies, J Mol Liq 283 (2019) 225-234.
550 [21] M. Taha, N.H. Ismail, W. Jamil, S. Imran, F. Rahim, S.M. Kashif, M. Zulkefeli, Synthesis
551 of 2-(2-methoxyphenyl)-5-phenyl-1, 3, 4-oxadiazole derivatives and evaluation of their
552 antiglycation potential, Med Chem Res 25(2) (2016) 225-234.
553 [22] T. Wang, K.B. Hicks, R. Moreau, Antioxidant activity of phytosterols, oryzanol, and other
554 phytosterol conjugates, J AM Oil Chem Soc 79(12) (2002) 1201-1206.
555 [23] C.-Y. Lo, S. Li, D. Tan, M.-H. Pan, S. Sang, C.-T. Ho, Trapping reactions of reactive

carbonyl species with tea polyphenols in simulated physiological conditions, Mol Nutr Food Res 50(12) (2006) 1118-1128.

[24] G.-x. Liu, Z.-c. Tu, W. Yang, H. Wang, L. Zhang, D. Ma, T. Huang, J. Liu, X. Li, Investigation into allergenicity reduction and glycation sites of glycated β-lactoglobulin with ultrasound pretreatment by high-resolution mass spectrometry, Food Chem 252 (2018) 99-107.

[25] I. Sadowska-Bartosz, I. Stefaniuk, S. Galiniak, G. Bartosz, Glycation of bovine serum albumin by ascorbate *in vitro*: Possible contribution of the ascorbyl radical?, Redox Biol 6 (2015) 93-99.

[26] A. Taha, T. Hu, Z. Zhang, A.M. Bakry, I. Khalifa, S. Pan, H. Hu, Effect of different oils and ultrasound emulsification conditions on the physicochemical properties of emulsions stabilized by soy protein isolate, Ultrason Sonochem 49 (2018) 283-293.

[27] I. Khalifa, R. Nie, Z. Ge, K. Li, C. Li, Understanding the shielding effects of whey protein on mulberry anthocyanins: Insights from multispectral and molecular modelling investigations, Int. J. Biol. Macromol 119 (2018) 116-124.

[28] N. Lu, L. Zhang, X. Zhang, J. Li, T.P. Labuza, P. Zhou, Molecular migration in high-protein intermediate-moisture foods during the early stage of storage: Variations between dairy and soy proteins and effects on texture, Food Res Int 82 (2016) 34-43.

[29] F. Putnam, The Plasma Proteins V3: Structure, Function, and Genetic Control, Elsevier (2012).

[30] Q. Xia, J. Chen, Y. Cao, R. Guan, H. Gao, Inhibitory Effect of Bayberry Polyphenols on Advanced Glycation End Products Formation, J of Chinese Institute of Food Sci and Tech 18(11) (2018) 13-21.

[31] K. Mohammed Khan, F. Rahim, N. Ambreen, M. Taha, M. Khan, H. Jahan, A. Shaikh, S.

579 Iqbal, S. Perveen, M. Iqbal Choudhary, Synthesis of benzophenonehydrazone Schiff bases and
580 their in vitro antiglycating activities, Med Chem 9(4) (2013) 588-595.
581 [32] M. Navarro, F.J. Morales, Evaluation of an olive leaf extract as a natural source of
582 antiglycative compounds, Food Res Int 92 (2017) 56-63.
583 [33] T. Suantawee, H. Cheng, S. Adisakwattana, Protective effect of cyanidin against glucose-
584 and methylglyoxal-induced protein glycation and oxidative DNA damage, I Int. J. Biol.
585 Macromol 93 (2016) 814-821.
586 [34] S. Arfin, G.A. Siddiqui, A. Naeem, S. Moin, Inhibition of advanced glycation end products
587 by isoferulic acid and its free radical scavenging capacity: An *in vitro* and molecular docking
588 study, Int. J. Biol. Macromol 118 (2018) 1479-1487.
589 [35] T.K. Girish, U.J. Prasada Rao, Protein glycation and aggregation inhibitory potency of
590 biomolecules from black gram milled by-product, J Sci Food Agric 96(15) (2016) 4973-4983.
591 [36] G. Prasanna, N. Saraswathi, Linolenic acid prevents early and advanced glycation end-
592 products (AGEs) modification of albumin, Int. J. Biol. Macromol 95 (2017) 121-125.
593 [37] L. Tang, S. Li, H. Bi, X. Gao, Interaction of cyanidin-3-O-glucoside with three proteins,
594 Food Chem 196 (2016) 550-559.
595 [38] H. Shen, Z. Gu, K. Jian, J. Qi, *In vitro* study on the binding of gemcitabine to bovine serum
596 albumin, J Pharmacut Biomed 75 (2013) 86-93.
597 [39] S. Jiang, M. Li, R. Chang, L. Xiong, Q. Sun, *In vitro* inhibition of pancreatic α-amylase by
598 spherical and polygonal starch nanoparticles, Food & Func 9(1) (2018) 355-363.
599 [40] U. Takahama, S. Hirota, Interactions of flavonoids with α-amylase and starch slowing down
600 its digestion, Food & Func 9(2) (2018) 677-687.
601 [41] J. Zhang, L. Xiao, Y. Yang, Z. Wang, G. Li, Lignin binding to pancreatic lipase and its

602 influence on enzymatic activity, Food Chem 149 (2014) 99-106.
603 [42] A. Belay, H.K. Kim, Y.-H. Hwang, Binding of caffeine with caffeic acid and chlorogenic
604 acid using fluorescence quenching, UV/vis and FTIR spectroscopic techniques, Luminescence
605 31(2) (2016) 565-572.
606 [43] J. Wei, D. Xu, X. Zhang, J. Yang, Q. Wang, Evaluation of anthocyanins in Aronia
607 melanocarpa/BSA binding by spectroscopic studies, AMB Express 8(1) (2018) 72.
608 [44] J. Yan, G. Zhang, J. Pan, Y. Wang, α-Glucosidase inhibition by luteolin: Kinetics,
609 interaction and molecular docking, Int. J. Biol. Macromol 64 (2014) 213-223.
610 [45] P.D. Ross, S. Subramanian, Thermodynamics of protein association reactions: Forces
611 contributing to stability, Biochemistry 20(11) (1981) 3096-3102.
612 [46] Y. Feng, F. Lu, X. Wu, Y. Li, Y. Shen, L. Fan, Z. He, K. Gao, Inhibitory potential of
613 phenylpropanoid glycosides from *Ligustrum purpurascens* Kudingcha against α-glucosidase and
614 α-amylase *in vitro*, Int J Food Sci Tech 50(10) (2015) 2280-2289.
615 [47] I. Khalifa, J. Peng, Y. Jia, J. Li, W. Zhu, X. Yu-juan, C. Li, Anti-glycation and anti-
616 hardening effects of microencapsulated mulberry polyphenols in high-protein-sugar ball models
617 through binding with some glycation sites of whey proteins, Int. J. Biol. Macromol 123 (2019)
618 10-19.
619 [48] M. Hosseini-Koupaei, B. Shareghi, A.A. Saboury, F. Davar, Molecular investigation on the
620 interaction of spermine with proteinase K by multispectroscopic techniques and molecular
621 simulation studies, Int. J. Biol. Macromol 94 (2017) 406-414.
622 [49] L. Zeng, G. Zhang, S. Lin, D. Gong, Inhibitory mechanism of Apigenin on α-glucosidase
623 and synergy analysis of flavonoids, J. Agric. Food Chem 64(37) (2016) 6939-6949.
624 [50] M. Skrt, E. Benedik, Č. Podlipnik, N.P. Ulrih, Interactions of different polyphenols with

bovine serum albumin using fluorescence quenching and molecular docking, Food Chem 135(4) (2012) 2418-2424.

[51] M.S. Ali, H.A. Al-Lohedan, Deciphering the interaction of procaine with bovine serum albumin and elucidation of binding site: A multi spectroscopic and molecular docking study, J Mol Liq 236 (2017) 232-240.

[52] S. Abbasi, S. Gharaghani, A. Benvidi, M. Rezaeinasab, New insights into the efficiency of thymol synergistic effect with p-cymene in inhibiting advanced glycation end products: A multi-way analysis based on spectroscopic and electrochemical methods in combination with molecular docking study. J Pharm Biomed Anal, 150, (2018) 436-451.

[53] D. J. Hinton, J. M. Ames, Site specificity of glycation and carboxymethylation of bovine serum albumin by fructose. Amino Acids, 30(4), (2006) 425-434.

Fig. 1. The chemical structure of the three phytosterols including β-sitosterol (A), stigmasterol (B), and gamma oryzanol (C) which were used in the current study.

Fig. 2. The dose-depend effects of SS, βS, and γO on the glucose-BSA binding ability (A), available lysine (B), fluorescent-AGEs and protein glycoxidation products (C), SDS-PAGE profiles of BSA-G without and with 0.1 mg mL^{-1} of SS, βS, and γO (D), the small rectangles were mad around BSA bands supplemented with their densitometric analysis, and their fluorescence microscopy digital micrographs (E), which were captured using an inverted microscopy (Nikon Eclipse Ti-S, Japan) at 10 x/0.25 magnification. The alphabet letters indicate a significant difference at $p<0.05$.

Fig. 3. The particle size distribution curves of bovine serum albumin with SS, βS, and γO complexes measured by DLS.

Fig. 4. The dose dependent effect (mg mL^{-1}) of SS, βS, and γO on the fluorescence spectra intensity of bovine serum albumin measured at λ_{ex}= 280 nm and λ_{em}= 290 - 450 nm. The Stern-Volmer plots for the quenching and the thermodynamic constants of BSA by each PS at different temperatures were also delivered at the upper and lower right-corner (λ_{ex}= 280 nm).

Fig. 5. The schematic diagram generated using the 2D and 3D diagram of Accelrys Discovery Studio shows the interactions between BSA with SS (A), βS (B), and γO (C) homology models.

Fig. 6. Effect of different concentrations (mg mL^{-1}) of SS, βS, and γO on the UV-vis absorbance of bovine serum albumin at λ = 225 - 750 nm.

Fig. 7. The whole FTIR spectra of bovine serum albumin influenced by interaction with the three phytosterols and their peak fit analysis of the range of 1300 -1700 cm^{-1} for bovine serum albumin conjugates with SS, βS, and γO.

Fig. 8. The CD spectrum of bovine serum albumin complexed with SS, βS, and γO (A), and their secondary structure elements (B), as well as their SDS-PAGE bands (C). Lanes 1, 2, 3, 4, and M are: BSA, BSA-SS, BSA-βS, BSA-γO, and marker, respectively. The red columns represented the densitometric analysis. The small rectangles were mad around BSA bands.

Fig. 9. The inhibitory effect of SS, βS, and γO on AGEs formation induced by hydroxyl radicals.